CrystEngComm

PAPER

View Article Online
View Journal | View Issue

Cite this: *CrystEngComm*, 2015, **17**, 3103

Decrease in particle size and enhancement of upconversion emission through Y^{3+} ions doping in hexagonal $NaLuF_4$:Yb^{3+}/Er^{3+} nanocrystals†

Guotao Xiang,[ab] Jiahua Zhang,*[a] Zhendong Hao,[a] Xia Zhang,[a] Guo-Hui Pan,[a] Yongshi Luo[a] and Haifeng Zhao[a]

Received 9th February 2015,
Accepted 12th March 2015

DOI: 10.1039/c5ce00294j

www.rsc.org/crystengcomm

The upconversion (UC) enhancement with size decrease has been realized through Y^{3+} ions doping in β-$NaLuF_4$:Yb^{3+}/Er^{3+} nanocrystals (NCs) by a solvothermal process. X-Ray diffraction (XRD), scanning electron microscopy (SEM) and UC luminescence spectra were used to characterize the resulting samples. With an increase of the Y^{3+} doping concentration, the NCs size is continuously decreased with no phase transition. Meanwhile, the UC intensity is firstly increased and then it decreases when the Y^{3+} ions concentration is over 30 mol%. The NCs (β-$NaLu_{0.48}Y_{0.3}Yb_{0.2}Er_{0.02}F_4$) with the optimum Y^{3+} ions doping concentration (30 mol%) for UC emission have a diameter of about 80 nm. Compared with β-$NaLu_{0.78}Yb_{0.2}Er_{0.02}F_4$ and β-$NaY_{0.78}Yb_{0.2}Er_{0.02}F_4$ prepared under the same conditions, the green UC emission is enhanced by a factor of 1.8 and 16, respectively, for β-$NaLu_{0.48}Y_{0.3}Yb_{0.2}Er_{0.02}F_4$. The variation of the UC intensity with the increasing Y^{3+} ions concentration is attributed to the changing of the symmetry of the local crystal field induced by Y^{3+} ions doping, which has been proved by the structural probe Eu^{3+} ions. For β-$NaLu_{0.78}Yb_{0.2}Er_{0.02}F_4$ and β-$NaLu_{0.48}Y_{0.3}Yb_{0.2}Er_{0.02}F_4$, a three-photon green UC process and a three-photon red UC process occur simultaneously at high pump power density, which can be described as $^4G_{11/2}$ (Er^{3+}) + $^4I_{15/2}$ (Er^{3+}) → $^2H_{11/2}$/$^4S_{3/2}$ (Er^{3+}) + $^4I_{13/2}$ (Er^{3+}) and $^4G_{11/2}$ (Er^{3+}) + $^2F_{7/2}$ (Yb^{3+}) → $^4F_{9/2}$ (Er^{3+}) + $^2F_{5/2}$ (Yb^{3+}), respectively.

Introduction

Lanthanide (Ln) ions co-doped UC NCs, which can be excited in the near-infrared (NIR) region to give emission in the visible region, have attracted much attention in recent years.[1–6] Such a unique luminescence mechanism has made the UC materials promising fluorophores in biological applications.[7–12] Under the excitation of low-energy NIR photons, the autofluorescence of biological samples and scattered excitation light could be eliminated; meanwhile, the NIR light has deeper imaging depth in tissues and causes much less photo-damage to living organisms.[13–18]

Considerable studies have shown that rare earth doped β-$NaYF_4$ is acknowledged as the most efficient UC host material because of its low photon energy (360 cm^{-1}).[19–21] As an important fluoride, β-$NaLuF_4$, with a similar structure to β-$NaYF_4$, may be a more promising host for UC behavior than β-$NaYF_4$ due to its unique electronic state at the top of the valence. Recently, Qin *et al.* have reported the intense ultraviolet and blue UC luminescence in β-$NaLuF_4$:Yb^{3+}/Tm^{3+} NCs with a diameter of about 180 nm.[22] However, such a large nanocrystal size restricts its biological applications. Up to now, there are only few papers in the literature concerning the size reduction of β-$NaLuF_4$.[23,33] Meanwhile, the UC luminescence intensity usually decreases with the reduced size because of the increased surface-to-volume ratio. It is a great challenge to combine small size and bright UC luminescence into one NC.

It is well established that the UC luminescence of rare earth doped materials is dependent on their intra 4f transition probabilities, which are significantly affected by the local crystal field symmetry.[24] Moreover, the worse the local crystal field symmetry is, the more intense the UC emission is. Impurity doping is an excellent method to break the symmetry of the local crystal field.[25] In addition, the substitution of ions with larger ionic radius favors the small size NCs, as predicted earlier.[23,26] Therefore, larger radius ions doping may be a promising way to enhance the UC intensity while reducing the size.

In this paper, we report the synthesis of β-$NaLu_{(0.78-x)}Y_xYb_{0.2}Er_{0.02}F_4$ (x = 0, 0.2, 0.3, 0.4, 0.5) NCs. The UC intensity

[a] *State Key Laboratory of Luminescence and Applications, Changchun Institute of Optics, Fine Mechanics and Physics, Chinese Academy of Sciences, Changchun 130033, Jilin, China. E-mail: zhangjh@ciomp.ac.cn; Fax: +86 431 8617 6317; Tel: +86 431 8617 6317*

[b] *Graduate School of Chinese Academy of Sciences, Beijing, 100039, China*

† Electronic supplementary information (ESI) available. See DOI: 10.1039/c5ce00294j

is firstly increased and then it decreases when the Y^{3+} ions concentration is over 30 mol%; but the NCs size continuous decreases with no phase transition with the increasing Y^{3+} doping concentration. Compared with β-$NaLu_{0.78}Yb_{0.2}Er_{0.02}F_4$ and β-$NaY_{0.78}Yb_{0.2}Er_{0.02}F_4$ prepared under the same conditions, the green UC emission is enhanced by a factor of 1.8 and 16, respectively, for β-$NaLu_{0.48}Y_{0.3}Yb_{0.2}Er_{0.02}F_4$. By using Eu^{3+} ions as the structural probe, the reason for the UC intensity changing with the increasing Y^{3+} ions concentration is presented. We also explored the UC properties of the prepared NCs.

Experimental

Chemicals

NaOH, NH_4F, HCl, methanol and ethanol were obtained from Beijing Chemical Reagent Company. Hexanes were obtained from Tianjin Guangfu Chemical Reagent Company. Lanthanide (Ln) oxides of SpecPure grade (Lu_2O_3, Y_2O_3, Yb_2O_3, Er_2O_3, Eu_2O_3, Ho_2O_3, Tm_2O_3, 99.99%), were purchased from Yangkou state-run rare earth company. 1-Octadecene (ODE, 90%) and oleic acid (OA, 90%) were supplied by Alfa Aesar. All of the chemical reagents were used as received without further purification. $LnCl_3$ was prepared by dissolving the corresponding lanthanide oxides in hydrochloric acid at an elevated temperature followed by evaporating the water under vacuum conditions.

Synthesis of β-$NaLu_{(0.78-x)}Y_xYb_{0.2}Er_{0.02}F_4$ (x = 0, 0.2, 0.3, 0.4, 0.5, 0.78) NCs

In a typical procedure, 1 mmol of $RECl_3$ (RE = (0.78 − x) Lu, 0.2 Yb, 0.02 Er, x Y, where x = 0, 0.2, 0.3, 0.4, 0.5, 0.78) was added to a 100 mL three-neck round-bottom flask containing ODE (15 mL) and OA (6 mL). The solution was magnetically stirred and heated to 140 °C for 30 min to form the lanthanide oleate complexes and remove residual water and oxygen. The temperature was then cooled to 50 °C with a gentle flow of argon gas through the reaction flask. Meanwhile, a solution of NH_4F (4 mmol) and NaOH (2.5 mmol) dissolved in methanol (10 mL) was added to the flask and the resulting mixture was stirred for 30 min to evaporate methanol from the reaction mixture; the temperature was then increased to 300 °C in an argon atmosphere for 90 min and then naturally cooled to room temperature. The resultant solid state products were precipitated by the addition of ethanol, collected by centrifugation, washed with ethanol three times, and finally redispersed in cyclohexane.

Synthesis of β-$NaLu_{(0.98-x)}Y_xEu_{0.02}F_4$ (x = 0, 0.2, 0.3, 0.4, 0.5) NCs

In a typical procedure, 1 mmol of $RECl_3$ (RE = (0.98 − x) Lu, 0.02 Eu, x Y, where x = 0, 0.2, 0.3, 0.4, 0.5) was added to a 100 mL three-neck round-bottom flask containing ODE (15 mL) and OA (6 mL). The solution was magnetically stirred and heated to 140 °C for 30 min to form the lanthanide oleate complexes and remove residual water and oxygen. The temperature was then cooled to 50 °C with a gentle flow of argon gas through the reaction flask. Meanwhile, a solution of NH_4F (4 mmol) and NaOH (2.5 mmol) dissolved in methanol (10 mL) was added to the flask and the resulting mixture was stirred for 30 min to evaporate methanol from the reaction mixture; the temperature was then increased to 300 °C in an argon atmosphere for 90 min and then naturally cooled to room temperature. The resultant solid state products were precipitated by the addition of ethanol, collected by centrifugation, washed with ethanol three times, and finally redispersed in cyclohexane.

Characterization

Powder X-ray diffraction (XRD) data were collected using Cu Kα radiation (λ = 1.54056 Å) on a Bruker D8 advance diffractometer equipped with a linear position-sensitive detector (PSD-50 m, M.Braun), operating at 40 kV and 40 mA with a step size of 0.01° (2θ) in the range of 10–70°. The morphology was investigated by using field emission scanning electron microscopy (SEM) (Hitachi S-4800). The UC spectra were measured using a FLS920 spectrometer (Edinburgh Instruments, UK) pumped with a power-controllable 980 nm diode laser. The emission spectrum under direct excitation was measured using a FLS920 spectrometer (Edinburgh Instruments, UK).

Results and discussion

Structure and morphology

The crystal structures and the phase purity of the as-prepared products were examined by XRD, as shown in Fig. 1(a). The positions and relative intensity of the diffraction peaks for β-$NaLu_{(0.78-x)}Y_xYb_{0.2}Er_{0.02}F_4$ (x = 0, 0.2, 0.3, 0.4, 0.5) NCs can be indexed well to the standard cards of the β-$NaLuF_4$ (JCPDS 27-0726). No second phase is detected in all XRD patterns except the diffraction peaks of NaCl, which are represented by the asterisk, demonstrating all the Y^{3+} ions are incorporated into the host matrix and formed a solid solution structure. Moreover, the diffraction peaks gradually broaden with increasing Y^{3+} ions, indicating a reduction of particle size, which is further verified by SEM observation. In addition, owing to the substitution of Lu^{3+} ions (radius = 0.85 Å) by the larger Y^{3+} ions (radius = 0.9 Å), the lattice constant and unit-cell volume increase with the increase in Y^{3+} ions concentration, resulting in the diffraction peaks shifting to low angles, which can be seen clearly by the red line in Fig. 1(a). The values of the lattice constant and unit-cell volumes were calculated according to XRD results and are shown in Table 1.

Fig. 1(b)–(f) shows the SEM images of β-$NaLu_{(0.78-x)}Y_xYb_{0.2}Er_{0.02}F_4$ (x = 0, 0.2, 0.3, 0.4, 0.5) NCs. The samples doped with different Y^{3+} ions concentration own the same morphology, displaying uniform hexagonal nanoplates. But the size of the NCs (listed in Table 1) decreases obviously with increasing Y^{3+} ions concentration. The changing of size can be attributed to the effect of the Y^{3+} ions dopant on crystal growth rate through surface charge modification, which

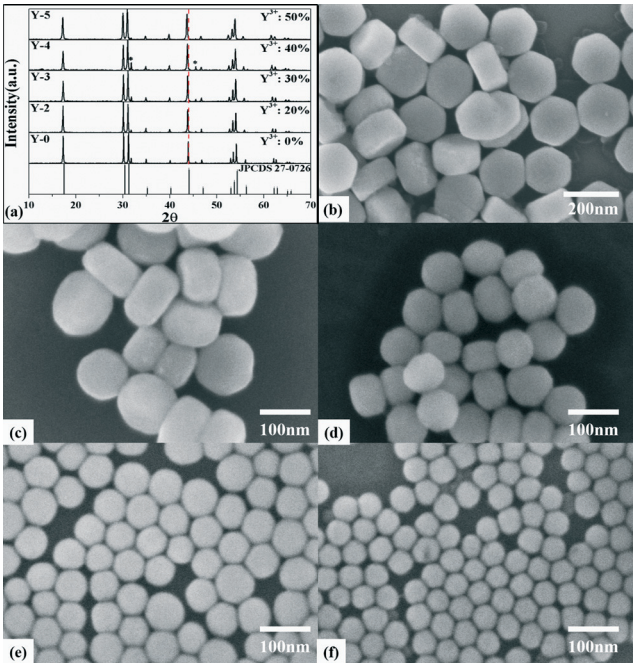

Fig. 1 (a) The standard XRD data of β-$NaLuF_4$ (JCPDS 27-0726) and the XRD patterns of β-$NaLu_{(0.78-x)}Y_xYb_{0.2}Er_{0.02}F_4$ (x = 0, 0.2, 0.3, 0.4, 0.5) NCs. The SEM images of β-$NaLu_{(0.78-x)}Y_xYb_{0.2}Er_{0.02}F_4$ NCs: (b) x = 0, (c) x = 0.2, (d) x = 0.3, (e) x = 0.4 and (f) x = 0.5. The diffraction peaks labelled by the asterisk are from NaCl.

Table 1 The lattice constants, unit-cell volumes and the NCs diameters of the β-$NaLuF_4$:Yb^{3+}/Er^{3+} NCs doped with different concentrations of Y^{3+} ions

Samples	a (Å)	c (Å)	Cell volume (Å^3)	NCs diameter (nm)
Y-0	5.9183	3.4597	104.94	200
Y-2	5.9288	3.4717	105.69	120
Y-3	5.9298	3.4787	105.93	80
Y-4	5.9316	3.4842	106.16	60
Y-5	5.9536	3.4857	107.0	40

has been proposed earlier.[26] More specifically, the electron charge density of the crystal surface increases after the Lu^{3+} ions are substituted by the larger radius ions Y^{3+} in the crystal lattice; then the change of electron charge density on the surface of the small sized NCs can sharply slow down the diffusion of negatively charged F^- ions to the surface, owing to the increase in charge repulsion, resulting in a tunable reduction of the NCs size.

Luminescence properties

Fig. 2 shows the normalized UC spectra of the as-prepared products pumped by a 980 nm diode laser. For the range from 500 nm to 600 nm, the spectra exhibit two emissions peaked around 520 nm and 540 nm, which are assigned to the $^2H_{11/2} \rightarrow {}^4I_{15/2}$ and $^4S_{3/2} \rightarrow {}^4I_{15/2}$ transitions of Er^{3+} ions, respectively. For the range from 600 nm to 700 nm, a red emission band around 650 nm is observed, which is assigned

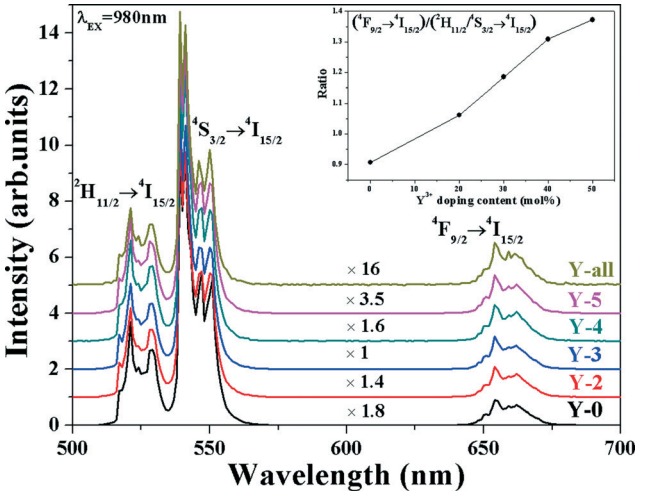

Fig. 2 The UC spectra of the resulting NCs under 980 nm excitation. Spectra are normalized to the maximum intensity of $^4S_{3/2} \rightarrow {}^4I_{15/2}$ transition. The inset is the intensity ratio of red to green obtained from the UC spectra.

to the $^4F_{9/2} \rightarrow {}^4I_{15/2}$ transition of Er^{3+} ions. It is noticed that the intensity of the UC emission is firstly increased and then decreases when the Y^{3+} ions concentration goes over 30 mol%. The green UC intensity of Y-3, with a diameter of about 80 nm, is 1.8 times stronger than that of Y-0, with a diameter of about 200 nm. That is to say, through Y^{3+} ions doping, the expected goal is realized for combining small size and bright UC luminescence into one NC. Moreover, 30 mol% is the optimum Y^{3+} ions doping concentration for UC emission. The inset of Fig. 2 is the intensity ratio of red UC emission to green UC emission obtained from the UC spectra. It displays an increasing red-to-green intensity ratio with the decreasing size. The enhancement of the nonradiative decays across the relevant energy gaps ($^4I_{11/2} \rightarrow {}^4I_{13/2}$ and $^4S_{3/2} \rightarrow {}^4F_{9/2}$) in smaller particles having a high surface-to-volume ratio is considered as the main factor for explaining this phenomenon.[27–29]

In order to further compare the UC properties, the β-$NaY_{0.78}Yb_{0.2}Er_{0.02}F_4$ NCs (named Y-all) were also synthesized under the same preparation conditions with a diameter of about 30 nm. The XRD, SEM and UC spectra of Y-all are shown in Fig. S1, S2† and 2, respectively. Investigated by UC spectra, the green UC intensity is 16 times stronger for Y-3 relative to Y-all. Meanwhile, despite the decrease of the UC intensity when the Y^{3+} concentration over 30 mol%, the green UC intensity of Y-5, which has a similar size to Y-all, is 4.6 times stronger than that of Y-all. These phenomena prove the excellent UC properties of β-$NaLu_{(0.78-x)}Y_xYb_{0.2}Er_{0.02}F_4$ (x = 0, 0.2, 0.3, 0.4, 0.5) NCs.

It is known that the $^5D_0 \rightarrow {}^7F_1$ transition of Eu^{3+} ions is of magnetic dipole nature, which is insensitive to the site symmetry; whereas the $^5D_0 \rightarrow {}^7F_2$ transition is of electric dipole nature and is very sensitive to the site symmetry. Therefore, the intensity ratio of the $^5D_0 \rightarrow {}^7F_2$ transition to the $^5D_0 \rightarrow {}^7F_1$ transition can act as an efficient fingerprint of local

symmetry for a luminescent center. In general, a higher ratio means a lower symmetry.[25,26] To explore the local symmetry of as-prepared samples, Eu^{3+} ions were taken as the structural probe to investigate the modification of the symmetry of the local crystal field induced by Y^{3+} ions doping. Fig. 3 shows the dependence of the intensity ratio (denoted as R) of the $^5D_0 \rightarrow {}^7F_2$ transition to the $^5D_0 \rightarrow {}^7F_1$ transition on Y^{3+} ions doping content in β-$NaLuF_4$: 0.02 Eu^{3+} NCs doped with different concentrations of Y^{3+} ions. The values of R show an initial increase followed by a decrease and reach a maximum at a 30 mol% concentration of Y^{3+} ions. The changing trend of R is the same as that of UC intensity in the corresponding samples. Therefore, it can be concluded that the variation of the UC intensity for Y^{3+} ions doped samples originates from the changing of symmetry around the rare earth ions.

The emission intensity of the photons depends upon laser pumping power as: $I \propto P^n$, where I is the visible output intensity, P is the infrared excitation power and n is the number of NIR photons absorbed per visible photon emitted, which can be determined from the slope of the linear plots between log(I) and log(P).[27] For any UC mechanism, although a two-photon process theoretically corresponds to a slope equal to approximately 2, the dependence of UC intensity on pump power is also expected to decrease the slope. Pollnau *et al.* attributed this phenomenon to the competition between linear decay and UC processes for the depletion of the intermediate exited states.[30] Lei *et al.* set up the steady-state luminescence dynamic equations considering a two-step energy transfer (ET) process and deduced that the UC intensity for a two-phonon ET process is proportional to the square of the excitation power density (P^2) when the linear decay of the intermediate state is dominant, while the intensity is proportional to the excitation power density (P^1) when the UC is the dominant mechanism in the Yb^{3+} and Er^{3+} codoped system.[31] In short, for any two-photon process, the intensity of an UC process that is excited by the sequential absorption of two photons has a dependence of P^n on absorbed pump power density P, with $1 < n < 2$. Fig. 4 shows the power dependence curves for the $^2H_{11/2}/{}^4S_{3/2} \rightarrow {}^4I_{15/2}$ transition and the $^4F_{9/2} \rightarrow {}^4I_{15/2}$ transition in Y-0 and Y-3 under 980 excitation wavelength, respectively. In the low pump power density (say < 2 mW mm^{-2} in this case), the slope n values for green and red emission are 1.75 and 1.64, respectively, in Y-0 and 1.6 and 1.59, respectively, in Y-3, indicating a two-photon process in each case, despite the n values deviating far from 2. In the high pump power density, however, the slope n values for green and red emission in both Y-0 and Y-3 are obviously increased. So we propose that a three-photon green UC process and a three-photon red UC process occur simultaneously at high pump power density, resulting in the increase of the corresponding n values, which can be described as $^4G_{11/2}$ (Er^{3+}) + $^4I_{15/2}$ (Er^{3+}) → $^2H_{11/2}/{}^4S_{3/2}$ (Er^{3+}) + $^4I_{13/2}$ (Er^{3+}) and $^4G_{11/2}$ (Er^{3+}) + $^2F_{7/2}$ (Yb^{3+}) → $^4F_{9/2}$ (Er^{3+}) + $^2F_{5/2}$ (Yb^{3+}), respectively.[15,32] Obviously, in both Y-0 and Y-3, the n value of the red UC process increases more effectively than that of the green UC process in the corresponding samples at high pump power density. This can be attributed to the high Yb^{3+} ions concentration and the low Er^{3+} ions concentration. As mentioned above, the three-photon green UC process is a cross-relaxation process between two Er^{3+} ions; however, the cross-relaxation in the three-photon red UC process is between Yb^{3+} ions and Er^{3+} ions. Since the Yb^{3+} ions concentration is much higher than the Er^{3+} ions concentration, the three-photon red UC process is more effective than the three-photon green UC process, resulting in a rapid increase of the n values of the red UC process. In addition, it should be noted that the amount of both the three-photon green UC process and the three-photon red UC process are very few, because of the enormous deviation of the n values from 3.[33]

Fig. 5 is the energy level diagram including various, mainly UC, mechanisms. Excited by 980 nm wavelength, Yb^{3+} was excited to the $^2F_{5/2}$ level by ground state absorption (GSA). For the two-photon green UC process, the two green emitting levels of $^2H_{11/2}$ and $^4S_{3/2}$ were populated by the sequential energy transfers ET(1) and ET(2), and the nonradiative relaxations $^4F_{7/2} \rightarrow {}^2H_{11/2}/{}^4S_{3/2}$. The two-photon population of the red emitting $^4F_{9/2}$ level was ascribed to the nonradiative relaxation process $^4I_{11/2} \rightarrow {}^2I_{13/2}$ and a subsequent ET(3) process; the nonradiative relaxation process $^2H_{11/2}/{}^4S_{3/2} \rightarrow {}^4F_{9/2}$ can also populate the $^4F_{9/2}$ level. For the

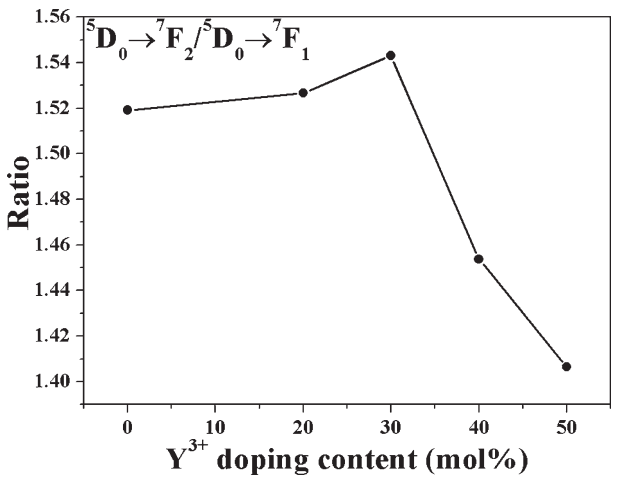

Fig. 3 The dependence of the intensity ratio of the $^5D_0 \rightarrow {}^7F_2$ transition to the $^5D_0 \rightarrow {}^7F_1$ transition on Y^{3+} doping content in β-$NaLuF_4$: 0.02 Eu^{3+} NCs doped with different concentrations of Y^{3+} ions.

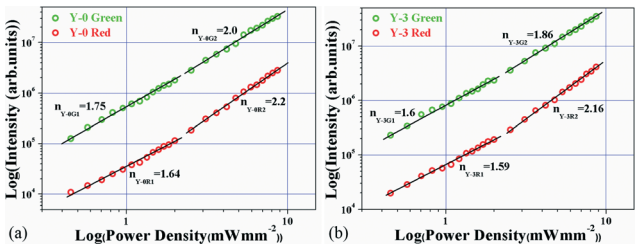

Fig. 4 The power dependence curves for the $^2H_{11/2}/{}^4S_{3/2} \rightarrow {}^4I_{15/2}$ transition and the $^4F_{9/2} \rightarrow {}^4I_{15/2}$ transition in (a) Y-0 and (b) Y-3 under 980 excitation wavelength.

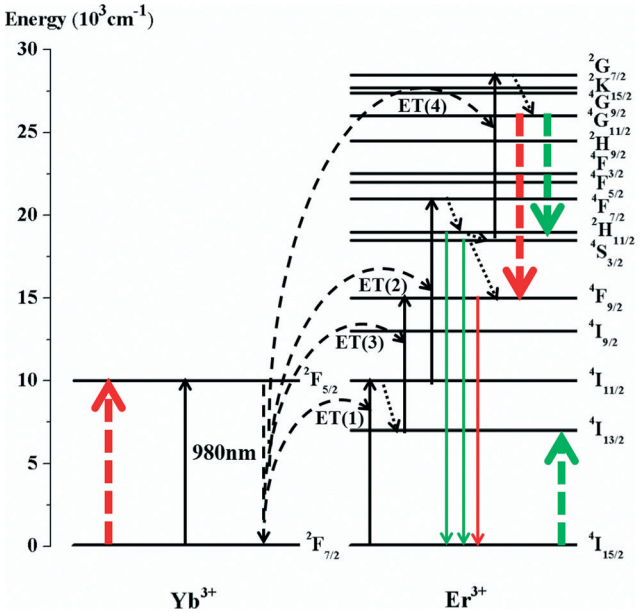

Fig. 5 The energy level diagrams and various, mainly UC, mechanisms in the prepared NCs following 980 nm excitation.

three-photon green and red UC processes, we suggest that the Er^{3+} ions in the $^4S_{3/2}$ level can be brought into the $^2G_{7/2}$ level by an ET(4) process followed by a nonradiative relaxation process to populate the $^4G_{11/2}$ level; then the Er^{3+} ions in the $^4G_{11/2}$ level can be de-excited to the $^2H_{11/2}/^4S_{3/2}$ levels or the $^4F_{9/2}$ level by the cross-relaxation processes mentioned above.

To further explore the properties of β-$NaLuF_4$ NCs by doping with Y^{3+} ions, we prepared β-$NaLu_{0.49}Y_{0.3}Yb_{0.2}Ho_{0.01}F_4$ and β-$NaLu_{0.49}Y_{0.3}Yb_{0.2}Tm_{0.01}F_4$ NCs. The XRD patterns and SEM images are shown in Fig. 6 and 7, respectively. The differences of the XRD patterns and SEM images for

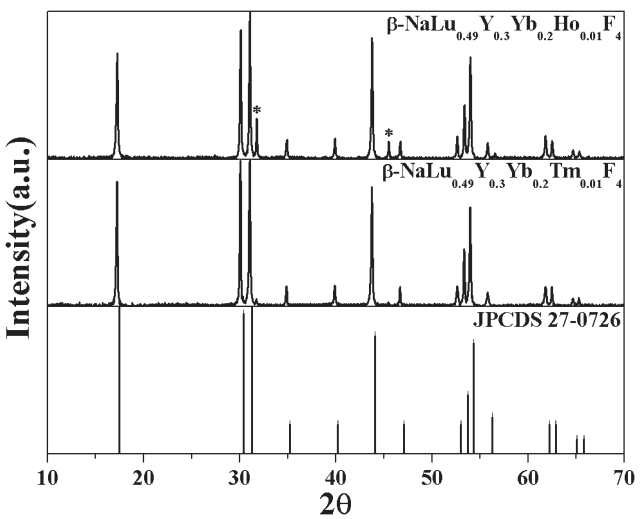

Fig. 6 The standard XRD data of β-$NaLuF_4$ (JCPDS 27-0726) and the XRD patterns of the β-$NaLu_{0.49}Y_{0.3}Yb_{0.2}Ho_{0.01}F_4$ and β-$NaLu_{0.49}Y_{0.3}Yb_{0.2}Tm_{0.01}F_4$ NCs. The diffraction peaks labelled by the asterisks are from NaCl.

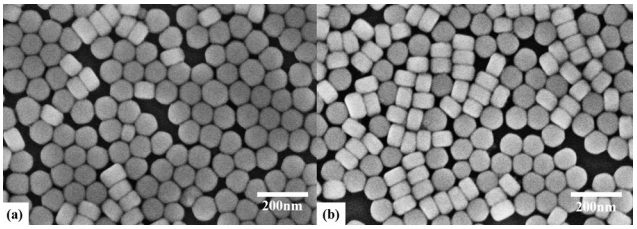

Fig. 7 The SEM images of (a) β-$NaLu_{0.49}Y_{0.3}Yb_{0.2}Ho_{0.01}F_4$ and (b) β-$NaLu_{0.49}Y_{0.3}Yb_{0.2}Tm_{0.01}F_4$.

β-$NaLu_{0.48}Y_{0.3}Yb_{0.2}Er_{0.02}F_4$, β-$NaLu_{0.49}Y_{0.3}Yb_{0.2}Ho_{0.01}F_4$ and β-$NaLu_{0.49}Y_{0.3}Yb_{0.2}Tm_{0.01}F_4$ are very few, which proves that the experimental results including phase, size and morphology have good reproducibility.

The UC emission spectra of β-$NaLu_{0.49}Y_{0.3}Yb_{0.2}Ho_{0.01}F_4$ and β-$NaLu_{0.49}Y_{0.3}Yb_{0.2}Tm_{0.01}F_4$ NCs excited by 980 nm wavelength with low output power density are shown in Fig. 8. For β-$NaLu_{0.49}Y_{0.3}Yb_{0.2}Ho_{0.01}F_4$, after an Yb^{3+} ion was excited to the $^2F_{5/2}$ state by 980 nm photons, its energy can be transferred to a nearby Ho^{3+} ion by the route of $^5I_8$ (Ho^{3+}) + $^2F_{5/2}$ (Yb^{3+}) → $^5I_6$ (Ho^{3+}) + $^2F_{7/2}$ (Yb^{3+}). A second Yb^{3+} ion in the $^2F_{5/2}$ state can also transfer its energy to the same Ho^{3+} ion that has been excited to the $^5I_6$ state, which can be raised to a higher-lying ($^5F_4/^5S_2$) state by the route of $^5I_6$ (Ho^{3+}) + $^2F_{5/2}$ (Yb^{3+}) → $^5F_4/^5S_2$ (Ho^{3+}) + $^2F_{7/2}$ (Yb^{3+}). The radiative transitions from $^5F_4/^5S_2$ to $^5I_8$ and $^5I_7$ levels result in the green emission centered at 540 nm and the emission centered at 749 nm, respectively. Nonradiative relaxation from the $^5F_4/^5S_2$ state of the Ho^{3+} ions may occur and populate the $^5F_5$ state, producing the red emission at 655 nm. For β-$NaLu_{0.49}Y_{0.3}Yb_{0.2}Tm_{0.01}F_4$, first, the Tm^{3+} ions in the ground state $^3H_6$ were excited to the excited state $^3H_5$ *via* an ET from neighboring Yb^{3+} ions. Subsequent non-radiative relaxation of $^3H_5$ → $^3F_4$ populated the $^3F_4$ level. Then the Tm^{3+} ions in $^3F_4$ state were excited to the $^3F_{2,3}$ states *via*

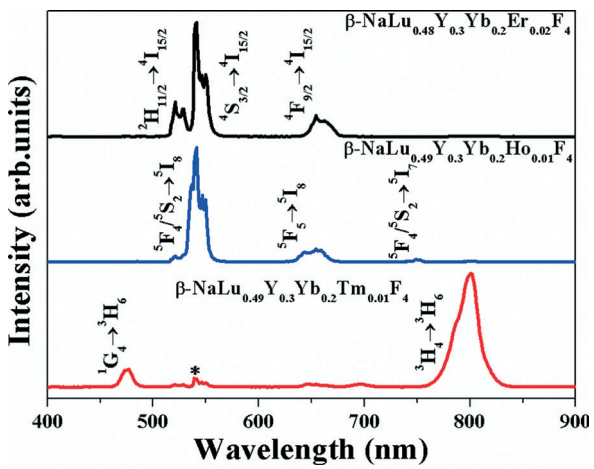

Fig. 8 The UC spectra of β-$NaLu_{0.48}Y_{0.3}Yb_{0.2}Er_{0.02}F_4$, β-$NaLu_{0.49}Y_{0.3}Yb_{0.2}Ho_{0.01}F_4$ and β-$NaLu_{0.49}Y_{0.3}Yb_{0.2}Tm_{0.01}F_4$ under 980 nm excitation. The emission band near 540 nm (labelled by the asterisk) is from a trace impurity of Ho^{3+}.

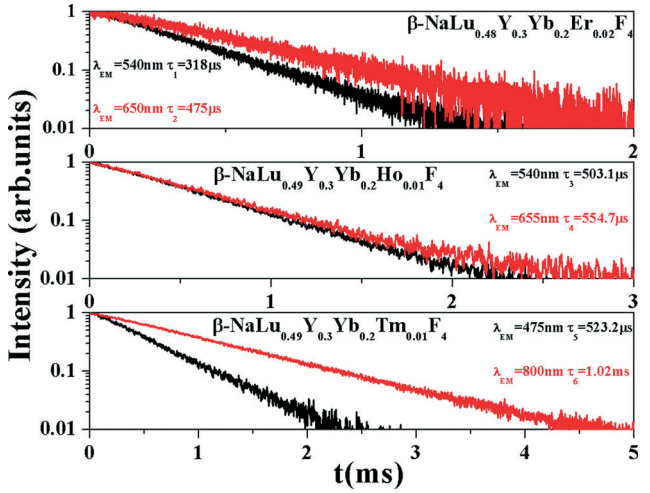

Fig. 9 The decay curves for Er^{3+}, Ho^{3+} and Tm^{3+} in β-$NaLu_{0.48}Y_{0.3}Yb_{0.2}Er_{0.02}F_4$, β-$NaLu_{0.49}Y_{0.3}Yb_{0.2}Ho_{0.01}F_4$ and β-$NaLu_{0.49}Y_{0.3}Yb_{0.2}Tm_{0.01}F_4$, respectively, under 980 excitation wavelength.

another ET from excited Yb^{3+} ions. The populated $^3F_{2,3}$ states may non-radiatively relax to the $^3H_4$ level and then produced 800 nm emission by the radiative transitions to the ground state $^3H_6$. Some of the Tm^{3+} ions in the $^3H_4$ state can be excited to the $^1G_4$ level *via* another ET from excited Yb^{3+} ions and then produced blue 475 nm emission.

Fig. 9 shows the decay curves for Er^{3+}, Ho^{3+} and Tm^{3+} in β-$NaLu_{0.48}Y_{0.3}Yb_{0.2}Er_{0.02}F_4$, β-$NaLu_{0.49}Y_{0.3}Yb_{0.2}Ho_{0.01}F_4$ and β-$NaLu_{0.49}Y_{0.3}Yb_{0.2}Tm_{0.01}F_4$, respectively, under 980 nm excitation wavelength. Excited by 980 nm wavelength, the decay times for the Er^{3+} $^4S_{3/2}$ level and $^4F_{9/2}$ level in β-$NaLu_{0.48}Y_{0.3}Yb_{0.2}Er_{0.02}F_4$, are 318 μs and 475 μs, respectively; the decay times for the Ho^{3+} $^5S_2$ level and $^5F_5$ level in β-$NaLu_{0.49}Y_{0.3}Yb_{0.2}Ho_{0.01}F_4$ are 503.1 μs and 554.7 μs, respectively; the decay times for the Tm^{3+} $^1G_4$ level and $^3H_4$ level in β-$NaLu_{0.49}Y_{0.3}Yb_{0.2}Tm_{0.01}F_4$ are 523.2 μs and 1.02 ms, respectively.

Conclusions

The UC enhancement with size decrease has been realized in β-$NaLuF_4$:Yb^{3+}/Er^{3+} NCs through doping with Y^{3+} ions. There was no phase transition during the Y^{3+} doping. The UC intensity firstly increases and then decreases, with the NCs size continuously decreasing, by increasing Y^{3+} doping concentration. 30 mol% doping concentration of Y^{3+} ions is found to be the optimum concentration for UC enhancement. Compared with Y-0 and Y-all prepared under the same conditions, the green UC emission is enhanced by a factor of 1.8 and 16, respectively, for Y-3. The change of the UC intensity with the increasing Y^{3+} ions concentration is attributed to the changing of the local symmetry around the luminescent centers, induced by Y^{3+} ions doping, which has been proved by the structural probe of Eu^{3+} ions. For Y-0 and Y-3, a three-photon green UC process and a three-photon red UC process occur simultaneously at high pump power density, which can be described as $^4G_{11/2}$ (Er^{3+}) + $^4I_{15/2}$ (Er^{3+}) → $^2H_{11/2}$/$^4S_{3/2}$ (Er^{3+}) + $^4I_{13/2}$ (Er^{3+}) and $^4G_{11/2}$ (Er^{3+}) + $^2F_{7/2}$ (Yb^{3+}) → $^4F_{9/2}$ (Er^{3+}) + $^2F_{5/2}$ (Yb^{3+}), respectively. Finally, we synthesized β-$NaLu_{0.49}Y_{0.3}Yb_{0.2}Ho_{0.01}F_4$ and β-$NaLu_{0.49}Y_{0.3}Yb_{0.2}Tm_{0.01}F_4$ NCs, demonstrating the good reproducibility of the experiments and the fitness of β-$NaLuF_4$ NCs synthesized by doping Y^{3+} ions for Ho^{3+} ions and Tm^{3+} ions doping.

Acknowledgements

This work is financially supported by the National Natural Science Foundation of China (51172226, 61275055, 11274007, 11174278, 51402284), the Natural Science Foundation of Jilin province (201205024, 20140101169JC) and the Youth Foundation of Jilin Province (20150520022JH).

Notes and references

1 H. X. Mai, Y. W. Zhang, R. Si, Z. G. Yan, L. D. Sun, L. P. You and C. H. Yan, *J. Am. Chem. Soc.*, 2006, **128**, 6426–6436.
2 K. A. Abel, J. C. Boyer and F. C. J. M. van Veggel, *J. Am. Chem. Soc.*, 2009, **131**, 14644–14645.
3 F. Auzel, *Chem. Rev.*, 2004, **104**, 139–173.
4 X. Teng, Y. H. Zhu, W. Wei, S. C. Wang, J. F. Huang, R. Naccache, W. B. Hu, A. I. Y. Tok, Y. Han, Q. C. Zhang, Q. L. Fan, W. Huang, J. A. Capobianco and L. Huang, *J. Am. Chem. Soc.*, 2012, **134**, 8340–8343.
5 W. P. Qin, Z. Y. Liu, C. N. Sin, C. F. Wu, G. S. Qin, Z. Chen and K. Z. Zheng, *Light: Sci. Appl.*, 2014, **3**, e193.
6 J. H. Zhang, Z. D. Hao, J. Li, X. Zhang, Y. S. Luo and G. H. Pan, *Light: Sci. Appl.*, 2015, **4**, e239.
7 Z. N. Wu, C. R. Guo, S. Liang, H. Zhang, L. P. Wang, H. C. Sun and B. Yang, *J. Mater. Chem.*, 2012, **22**, 18596–18602.
8 G. C. Jiang, J. Pichaandi, N. J. J. Johnson, R. D. Burke and F. C. J. M. van Veggel, *Langmuir*, 2012, **28**, 3239–3247.
9 S. S. Cui, H. Y. Chen, H. Y. Zhu, J. M. Tian, X. M. Chi, Z. Y. Qian, S. Achilefuc and Y. Q. Gu, *J. Mater. Chem.*, 2012, **22**, 4861–4873.
10 G. F. Wang, Q. Peng and Y. D. Li, *Acc. Chem. Res.*, 2011a, **44**, 322–332.
11 E. M. Dianov, *Light: Sci. Appl.*, 2012, **1**, e12.
12 D. K. Chatterjee, M. K. Gnanasammandhan and Y. Zhang, *Small*, 2010, **6**, 2781–2795.
13 Z. L. Wang, J. H. Hao, H. L. W. Chan, G. L. Law, W. T. Wong, K. L. Wong, M. B. Murphy, T. Su, Z. H. Zhang and S. Q. Zeng, *Nanoscale*, 2011b, **3**, 2175–2181.
14 M. X. Yu, F. Y. Li, Z. G. Chen, H. Hu, C. Zhan, H. Yang and C. H. Huang, *Anal. Chem.*, 2009, **81**, 930–935.
15 H. X. Mai, Y. W. Zhang, L. D. Sun and C. H. Yan, *J. Phys. Chem. C*, 2007, **111**, 13721–13729.
16 D. M. Yang, C. X. Li, G. G. Li, M. M. Shang, X. J. Kang and J. Lin, *J. Mater. Chem.*, 2011, **21**, 5923–5927.
17 F. Shi, J. S. Wang, D. S. Zhang, G. S. Qin and W. P. Qin, *J. Mater. Chem.*, 2011a, **21**, 13413–13421.
18 R. A. Jalil and Y. Zhang, *Biomaterials*, 2008, **29**, 4122–4128.

19 Z. Q. Li and Y. Zhang, *Nanotechnology*, 2008, **19**, 345606.
20 K. W. Krämer, D. Biner, G. Frei, H. U. Güdel, M. P. Hehlen and S. R. Lüthi, *Chem. Mater.*, 2004, **16**, 1244–1251.
21 Y. Wei, F. Q. Lu, X. R. Zhang and D. P. Chen, *Chem. Mater.*, 2006, **18**, 5733–5737.
22 F. Shi, J. S. Wang, X. S. Zhai, D. Zhao and W. P. Qin, *CrystEngComm*, 2011b, **13**, 3782–3787.
23 Q. Liu, Y. Sun, T. S. Yang, W. Feng, C. G. Li and F. Y. Li, *J. Am. Chem. Soc.*, 2011, **133**, 17122–17125.
24 Q. M. Huang, J. C. Yu, E. Ma and K. M. Lin, *J. Phys. Chem. C*, 2010, **114**, 4719–4724.
25 L. Lei, D. Q. Chen, P. Huang, J. Xu, R. Zhang and Y. S. Wang, *Nanoscale*, 2013, **5**, 11298–11305.
26 F. Wang, Y. Han, C. S. Lim, Y. H. Lu, J. Wang, J. Xu, H. Y. Chen, C. Zhang, M. H. Hong and X. G. Liu, *Nature*, 2010, **463**, 1061–1065.
27 F. Vetrone, J. C. Boyer, J. A. Capobianco, A. Speghini and M. Bettinelli, *J. Appl. Phys.*, 2004, **96**, 661–667.
28 Y. Wang, L. P. Tu, J. W. Zhao, Y. J. Sun, X. G. Kong and H. Zhang, *J. Phys. Chem. C*, 2009, **113**, 7164–7169.
29 J. B. Zhao, Z. D. Lu, Y. D. Yin, C. McRae, J. A. Piper, J. M. Dawes, D. Y. Jin and E. M. Goldys, *Nanoscale*, 2013, **5**, 944–952.
30 M. Pollnau, D. R. Gamelin, S. R. Lüthi and H. U. Güdel, *Phys. Rev. B: Condens. Matter Mater. Phys.*, 2000, **61**, 3337–3346.
31 Y. Q. Lei, H. W. Song, L. M. Yang, L. X. Yu, Z. X. Liu, G. H. Pan, X. Bai and L. B. Fan, *J. Chem. Phys.*, 2005, **123**, 174710.
32 C. Wright, *Top. Appl. Phys.*, 1976, **15**, 239–295.
33 G. T. Xiang, J. H. Zhang, Z. D. Hao, X. Zhang, Y. S. Luo, S. Z. Lü and H. F. Zhao, *CrystEngComm*, 2014, **16**, 2499–2507.